ACS OMEGA

http://pubs.acs.org/journal/acsodf

Review

Stable Assemblies of Topological Defects in Nematic Orientational Order

Arbresha Hölbl, Luka Mesarec, Juš Polanšek, Aleš Iglič, and Samo Kralj*

Cite This: *ACS Omega* 2023, 8, 169–179

Read Online

ACCESS | Metrics & More | Article Recommendations

ABSTRACT: We considered general mechanisms enabling the stabilization of localized assemblies of topological defects (TDs). There is growing evidence that physical fields represent fundamental natural entities, and therefore these features are of interest to all branches of physics. In general, cores of TDs are energetically costly, and consequently, assemblies of TDs are unfavorable. Owing to the richness of universalities in the physics of TDs, it is of interest to identify systems where they are easily experimentally accessible, enabling detailed and well-controlled analysis of their universal behavior, and cross-fertilizing knowledge in different areas of physics. In this respect, thermotropic nematic liquid crystals (NLCs) represent an ideal experiment testbed for such studies. In addition, TDs in NLCs could be exploited in several applications. We present examples that emphasize the importance of curvature imposed on the phase component of the relevant order parameter field. In NLCs, it is represented by the nematic tensor order parameter. Using a simple Landau-type approach, we show how the coupling between chirality and saddle splay elasticity, which can be expressed as a Gaussian curvature contribution, can stabilize Meron TDs. The latter have numerous analogs in other branches of physics. TDs in 2D curved manifolds reveal that the Gaussian curvature dominantly impacts the assembling and stabilization of TDs. Furthermore, a strong enough curvature that serves as an attractor for TDs is a respective field that could be imposed in a fast enough phase transition. Assemblies of created TDs created in such a disordered environment could be stabilized by appropriate impurities.

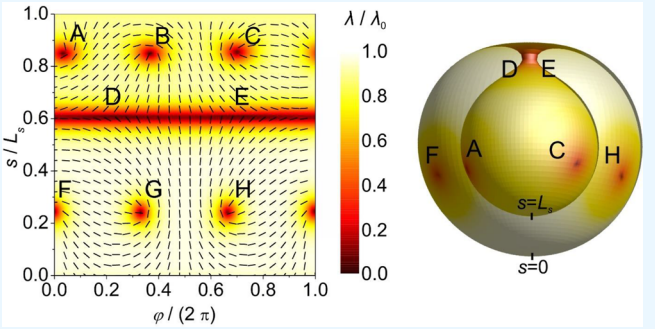

1. INTRODUCTION

Continuous symmetry breaking phase transitions are ubiquitous in nature and appear at all length scales, including particle physics, condensed matter systems, and cosmology.[1] To describe the essential properties of the resulting broken phase one should identify the broken symmetry and examine its elementary excitations and topological defects.[2] For this purpose, Landau-type approaches are particularly convenient, in which the broken phase configuration is presented by an order parameter field.[3] The modeling is based on symmetry and topology, for which a microscopic system's details are of secondary importance. This is fingerprinted in the emergent rich pallet of universal behaviors. Furthermore, it seems that physical fields might constitute fundamental natural entities.[4] Interpreting natural phenomena from this perspective might unveil several unresolved fundamental problems in understanding nature. For example, hot topics of constant interest for decades include the intriguing behavior of neutrinos and the origin of dark matter and dark energy; physicists are still struggling to fully understand the proton.[5] In these phenomena, localized field structures[6] might play an important role. To study in detail universal behaviors, it is of interest to identify experimentally accessible systems where such features could be studied in detail. Gained knowledge might shed light on behavior of their analogs in related systems, which are otherwise hardly experimentally accessible.[7]

Landau-type modeling of symmetry-breaking phase transitions introduces order parameter fields describing order in the broken phase. In general, an order parameter field consists of two qualitatively different components:[8] *amplitude* fields and *phase* fields. *Amplitude* fields measure the strength of established order and are in bulk equilibrium characterized by a single value. In the absence of external ordering fields, they equal zero in the higher symmetry phase. *Phase* fields determine the symmetry breaking system's choice among an infinitely degenerate set of competing states. This degeneracy enables long-range forces and topological defects (TDs). The latter corresponds to topologically protected localized order

Received: November 7, 2022
Accepted: December 7, 2022
Published: December 20, 2022

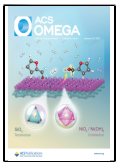

https://doi.org/10.1021/acsomega.2c07174
ACS Omega 2023, 8, 169–179

parameter configurations.[9] TDs are classified using group theory approaches. For this purpose, order parameter manifold $\mathcal{M}_0$ is introduced,[8] consisting of all equilibrium order parameter *phase* configurations. For example, the existence of the topologically protected wall, line, or point TDs is reflected in nontrivial homotopic groups[7,10] $\pi_0(\mathcal{M}_0)$, $\pi_1(\mathcal{M}_0)$, and $\pi_2(\mathcal{M}_0)$, respectively. These defect configurations are commonly described by conserved topological charges which are topological invariants.

Liquid crystal (LC) phases represent an ideal laboratory system to study the general physics of order parameter excitations.[8,11] They consist of relatively weakly interacting anisotropic molecules. Weak mutual couplings allow fast noncollective fluctuations which efficiently average out microscopic details. The resulting mesoscopic orientational order is described by molecular fields exhibiting in general *p*-atic order[12,13] (e.g., cases $p = 1$ and $p = 2$ can be described by vector and line fields, respectively). The orientational order is in several LC phases accompanied also by translational order. Resulting configurations possess a unique combination of liquid character, orientational and/or translational order, softness (capability to respond strongly to even weak stimuli), optical anisotropy, and optical transparency. This extraordinary symbiosis of properties allows relative ease of experimental observations.[11,14] In particular, owing to optic anisotropy, order parameter excitations could be monitored using simple optic polarization microscopy.[10,15−20] Furthermore, a rich pallet of existing LC phases possesses analogs of almost all physical phenomena. For example, smectic A (SmA) configurations bear some resemblance to superconductors[21] and Abrikosov lattices,[22] coarsening dynamics of defect structures in a fast enough isotropic−nematic (I−N) quenches provides clues of the early universe evolution,[15,23] and studies of topological defects[7,10,16,17,24] and knots[18,20] in LCs give insight into particle-like excitations in nature.

In this paper, we consider excitations in relatively simple achiral and chiral nematic thermotropic LC phases. They can be reached on cooling from the isotropic, i.e., ordinary, liquid phase. For illustration ease, we consider rod-like LC molecules. Their local orientational order is at the mesoscopic level commonly described by the tensor nematic order parameter[8] $\mathbf{Q}$. In bulk equilibrium it, can be expressed in terms of the scalar uniaxial order parameter $S \in [-1/2,1]$ (*amplitude* field) and pseudovector $\mathbf{n}$ (*phase* field), where states $\pm\,\mathbf{n}$ are physically equivalent. The unit vector $\mathbf{n}$, also referred to as the nematic director field, points along the local uniaxial direction. In the achiral nematic phase, $\mathbf{Q}$ is spatially homogeneous. In the chiral LCs, various structures can appear, which include the helical cholesteric phase and different blue phases.[8] The order parameter phase space[8] $\mathcal{M}_0$ equals the two-sphere with antipodal points identified (S_2/Z_2). Its homotopy reads $\pi_1(\mathcal{M}_0) = Z_2$ and $\pi_2(\mathcal{M}_0) = Z$, while $\pi_0(\mathcal{M}_0)$ is trivial. Therefore, these systems can exhibit topologically protected line and point defects. On the other hand, the wall defect could be stabilized only due to energy reasons.

2. MESOSCOPIC MODEL

We focus on bulk thermotropic achiral and chiral uniaxial LCs. We also consider cases where LC is manipulated by an external electric field $\mathbf{E}$. In the frame of the Landau−de Gennes mesoscopic model, one commonly expresses the free energy functional in terms of the traceless and symmetric tensor nematic order parameter[8]

$$\mathbf{Q} = \sum_{i=1}^{3} \mathbf{s}_i \mathbf{e}_i \otimes \mathbf{e}_i \tag{1}$$

Here, $\mathbf{s}_i$ stands for the *amplitude* fields ($\mathbf{Q}$ eigenvalues) and $\mathbf{e}_i$ are the *phase* fields (normalized eigenvectors of $\mathbf{Q}$). In the case of uniaxial order, $\mathbf{Q}$ is simplified to

$$\mathbf{Q} = S(\mathbf{n} \otimes \mathbf{n} - \mathbf{I}/3) \tag{2}$$

2.1. Free Energy. We express the free energy density $f = f_c + f_e + f_f$ as a sum of condensation (f_c), elastic (f_e), and external ordering field (f_f) contributions:[8,25]

$$f_c = \frac{3a_0}{2}(T - T^*)Tr\mathbf{Q}^2 - \frac{9b}{2}Tr\mathbf{Q}^3 + \frac{9c}{4}(Tr\mathbf{Q}^2)^2 \tag{3a}$$

$$f_e = \frac{L}{2}|\nabla\mathbf{Q}|^2 + 2q_0 L\mathbf{Q}\cdot\nabla\times\mathbf{Q} \tag{3b}$$

$$f_f = \frac{\Delta\varepsilon\varepsilon_0}{3}\mathbf{E}\cdot\mathbf{Q}\mathbf{E} \tag{3c}$$

We included only the most essential symmetry allowed terms to describe phenomena of our interest. Numerical coefficients are introduced for later convenience. The condensation term determines the local amplitude S imposed by inherent LC properties. These are defined by positive phenomenological material parameters a_0, b, c, and T^*. The term enforces first order phase transition at $T_{IN} = T^* + \frac{b^2}{4a_0c}$, where the equilibrium value of S is given by $S_{eq}(T \le T_{IN}) = \frac{S_0}{4}\left(3 + \sqrt{9 - 8\frac{T - T^*}{T_{IN} - T^*}}\right)$ and $S_{eq}\ (T > T_{IN}) = 0$, where $S_0 = S_{eq}(T_{IN}) = \frac{b}{2c}$. LC elasticity is approximated by a single positive elastic constant L. q_0 represents the LC inherent chirality wave vector. ε_0 is the vacuum permittivity, and $\Delta\varepsilon$ measures the dielectric anisotropic response in an external electric field $\mathbf{E}$. We limit to LCs exhibiting positive anisotropies, where $\mathbf{n}$ tends to be aligned along $\mathbf{E}$. One commonly assumes that the material quantities described above are temperature independent.

The model is characterized by numerous material-dependent lengths. For later convenience, we introduce the uniaxial (ξ) and biaxial (ξ_b) coherence lengths.[8,11] In the nematic phase, they are expressed as

$$\xi = \sqrt{L/\frac{\partial^2 f_c^{(eq)}}{\partial S^2}},\ \xi_b = \sqrt{L/(bS_{eq})} \tag{4}$$

2.2. Nematic Director Field Distortions. Let us focus on the nematic director field excitations which are, in general, relatively easily (i.e., the corresponding energy costs are low) established. It has been recently shown that the tensor gradient $\nabla\mathbf{n}$ can be decomposed into four fundamental modes,[26,27] referred to as the *bend*, *double splay*, *double twist*, and *tetrahedral splay* modes. Each of these modes could be separately excited.

The classical Oseen−Frank free energy[9,26] is expressed as a sum of symmetry-allowed terms:

https://doi.org/10.1021/acsomega.2c07174
ACS Omega 2023, 8, 169−179

$$f_e = \frac{K_{11}}{2}(\nabla\cdot\mathbf{n})^2 + \frac{K_{22}}{2}(\mathbf{n}\cdot\nabla\times\mathbf{n} - q_0)^2 + \frac{K_{33}}{2}|\mathbf{n}\times\nabla\times\mathbf{n}|^2 - K_{24}\nabla\cdot(\mathbf{n}\nabla\cdot\mathbf{n} + \mathbf{n}\times\nabla\times\mathbf{n}) \quad (5)$$

weighted by temperature-dependent Frank splay (K_{11}), twist (K_{22}), bend (K_{33}), and saddle-splay (K_{24}) elastic constants. However, these terms are generally coupled. The saddle splay distortions in general includes also splay and twist distortion. In particular, this contribution plays a particularly important role concerning topology. Namely, the saddle splay term can be expressed[8] as the Gaussian curvature K_g of a small surface patch whose surface normal points along $\mathbf{n}$:

$$\nabla\cdot(\mathbf{n}\nabla\cdot\mathbf{n} + \mathbf{n}\times\nabla\times\mathbf{n}) = 2K_g \quad (6)$$

In pioneering studies, this term has been commonly discarded because it can be transformed into the surface enclosing the LC body. It has been expected that for strong enough surface anchoring the anchoring contribution is dominating at the surface, overshadowing the saddle-splay contribution. However, this term determines volume LC elastic properties. By neglecting it, we discard possibilities to stabilize topological defects,[28] as will be shown in the following. In particular, we will illustrate that the Gaussian curvature plays an essential role in the physics of TDs.

2.3. Topological Excitations. As the simplest illustration, we first consider an achiral two-dimensional (2D) nematic where LC behavior is dictated only by the condensation and elastic free energy penalties. In the (x,y) Cartesian plane, we use parametrization $\mathbf{n} = \mathbf{e}_x\cos\theta + \mathbf{e}_y\sin\theta$ and assume spatially homogeneous uniaxial order. The unit vectors $(\mathbf{e}_x,\mathbf{e}_y)$ point along the Cartesian (x,y) coordinates. Solutions to the equilibrium Euler−Lagrange equation $\nabla^2\theta = 0$ read:[8]

$$\theta = m\varphi + \theta_0 \quad (7)$$

Here, $\varphi = \arctan\left(\frac{y}{x}\right)$, m stands for the winding number, and θ_0 is a constant. Structures with $m = 0$ describe equilibrium spatially homogeneous nematic configurations where the symmetry breaking direction is given by θ_0. Furthermore, cases $m \neq 0$ correspond to topological defects centered at $(x,y) = 0$. Due to head-to-tail invariance of $\mathbf{n}$, the winding number can exhibit half integers. In 2D, m plays the role of topological charge, which is a topological invariant. Conservation of m dictates merging, decaying, and transformations of TDs. TDs bearing $m > 0$ and $m < 0$ are commonly referred to as *defects* and *antidefects*, respectively. Figure 1a depicts an $m = 1$ defect. In general, TDs exhibiting a minimal value of m (i.e., $|m| = 1/2$) can be locally stable,[8,29,30] and defect pairs $\{-m,m\}$ in the nematic phase tend to annihilate into a defectless state. In Figure 1b, we show a defect pair $\{1/2, -1/2\}$, which could be induced by a local thermal fluctuation, prior to annihilation. On increasing the temperature above T_{IN}, numerous pairs $\{1/2, -1/2\}$ are formed, where their mutual interaction is overshadowed by thermal fluctuations. The resulting "gas" of TDs corresponds to the isotropic phase.[31] A representative time snapshot, where several pairs are present, is shown in Figure 1d.

In 2D, only point defects are possible. In 3D, in addition, line defects (disclinations) are ubiquitous.[8,23,32] These can either form closed loops[9,33−37] or originate and terminate at an LC limiting substrate.[9,11,38,39] In 3D, one assigns to TDs in addition to winding number (which reveals the local structure of disclinations) also 3D integer topological charge q, which is an integer. It is defined[10,40,41] by an integral over a closed surface parametrized by variables u and v:

$$q = \frac{1}{4\pi}\oint\oint \mathbf{n}\cdot\frac{\partial\mathbf{n}}{\partial u}\times\frac{\partial\mathbf{n}}{\partial v}\,du\,dv \quad (8)$$

Note that the sign of q is not uniquely defined due to the head-to-tail invariance of $\mathbf{n}$.

A closed loop of a wedge disclination, which is locally defined by winding number $m = 1/2$ or $m = -1/2$, bears topological charge $|q| = 1$. On the other hand, the twist disclination, in which the winding number switches the sign of m, holds $q = 0$ (i.e., it is chargeless). Therefore, the far director field of a closed wedge disclination resembles that of a point defect of charge $|q| = 1$. An example is schematically sketched in Figure 2a. On the other hand, the far field of an isolated closed twist disclination is essentially spatially homogeneous. Due to their chargeless character twist, disclination loops are not topologically stable.

In nematics, wall defects could be stabilized only energetically (i.e., not topologically) by imposing contradicting orientational order on distances comparable to the biaxial coherence length.[42,43] Furthermore, to avoid singularity at the centers of defects their cores[35,44,45] locally enter either isotropic or biaxial states.

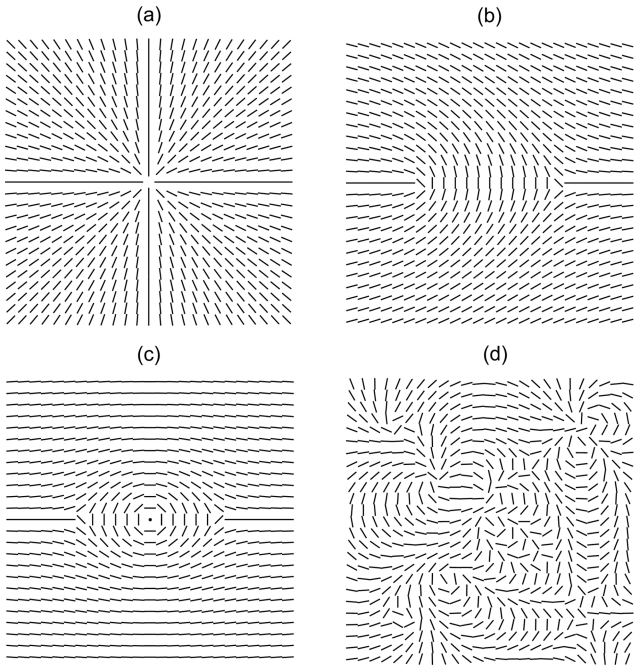

Figure 1. Characteristic director field of nematic point defects in 2D. (a) $m = 1$ defect. (b) Pair of defects $\{1/2, -1/2\}$. (c) An assembly of three defects $\{-1/2, 1, -1/2\}$. (d) An example of numerous defects which are excited by strong enough thermal fluctuations. In cases b and c, the far nematic director field is essentially spatially homogeneous.

3. RESULTS

In the following, we demonstrate key TD creation and stabilization mechanisms. Note that, in general, bulk nematic equilibrium tends to be defectless. Namely, the cores of TDs are, in general, energetically expensive, and furthermore $q \neq 0$ fingerprints elastic distortions in $\mathbf{n}$.

3.1. Chirality and Saddle-Splay Imposed Stabilization. In Figure 1c, we show a 2D assembly of three defects

https://doi.org/10.1021/acsomega.2c07174
ACS Omega 2023, 8, 169−179

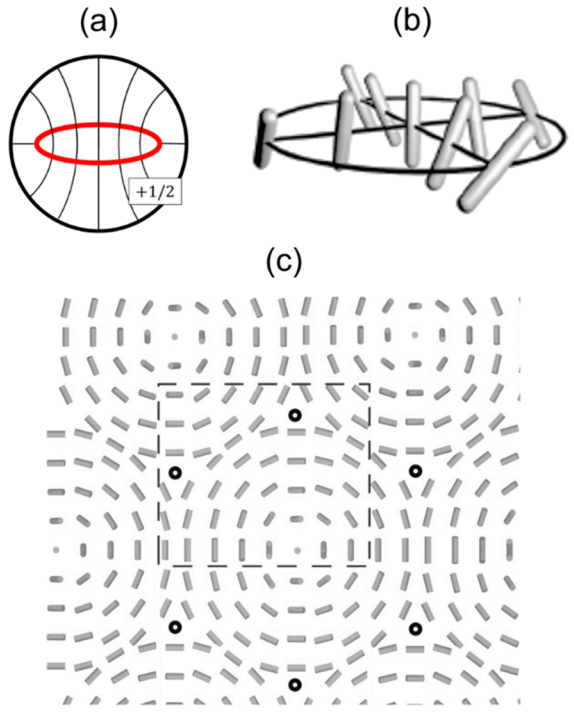

Figure 2. (a) The far field of a closed $m = 1/2$ disclination loop (red line) resembles the director field of the $q = 1$ hedgehog point defect. This nematic structure is commonly stabilized in LCs confined within a droplet, whose surface imposes a homeotropic anchoring condition (i.e., **n** is aligned along the local surface normal direction). (b) Sketch of the DT local structure close to the cylindrical symmetry axis of the excitation. (c) Schematic structure of a lattice of merons within the x/y plane. The dashed rectangle represents a chargeless region. It consists of an escaped $m = 1$ nonsingular structure and two singular $m = -1/2$ defects.

bearing topological charges $\{m = -1/2, m = 1, m = -1/2\}$ so that the total charge of the system equals zero. Under what conditions could this or a similar assembly be stable? Note that this three-component "quasi-particle" roughly resembles a neutron (i.e., its electric charge is zero, and it consists of three charged quarks).

In the following, we illustrate that a similar assembly could be stabilized in chiral 3D LCs in merons,[46] members of the skyrmion[6,24,28] family. For this purpose, we consider the double twist[27,28] nematic director field excitations. Locally, the corresponding **n** is roughly approximated in the cylindrical coordinate system (ρ, φ, z) by[46]

$$\mathbf{n} = -\mathbf{e}_{\varphi}\sin(Q\rho) + \mathbf{e}_{z}\cos(Q\rho) \tag{9}$$

where the double-twist (DT) periodicity Q is a variational parameter. The nematic distortion of this elastic mode nearby the symmetry axis at $\rho = 0$ is depicted in Figure 2b. To estimate the equilibrium value of Q, we calculate the free energy penalty of the DT solution, eq 9, within a cylinder of length h and radius $R = \frac{\pi}{2Q}$ (i.e., $\mathbf{n}(\rho = R) = -\mathbf{e}_{\varphi}$). The corresponding free energy reads

$$f_e = \frac{K_{22}}{2}\left(q_0 - Q - \frac{\sin(2Q\rho)}{2\rho}\right)^2 + \frac{K_{33}}{2}\frac{\sin^4(Q\rho)}{\rho^2} - K_{24}\frac{Q}{\rho}\sin(2Q\rho) \tag{10}$$

The DT saddle-splay penalty is given by

$$F_{24} = -2\pi K_{24} h \sin^2(QR) = -2\pi K_{24} h \tag{11}$$

Therefore, the saddle splay elasticity promotes DT excitation for $K_{24} > 0$. Of interest to us is obtaining conditions that minimize the free energy penalty $f_{DT} = \frac{1}{V}2\pi h\int_0^R f_e \rho\, d\rho$ of DT solution per LC volume $V = \pi R^2 h$. In terms of dimensionless quantities $\mu = \frac{Q}{q_0}$, $k_3 = \frac{K_{33}}{K_{22}}$, $k_{24} = \frac{K_{24}}{K_{22}}$, and $x = \frac{\rho}{R}$, one calculates $f_{DT}(\mu)$, which is minimized for $\mu_{min} \equiv \frac{Q_{min}}{q_0}$. It follows that

$$\mu_{min} = (4 + \pi^2)/\Big(8 + \text{EulerGamma}(1 + 3k_3) - 16k_{24} + \pi^2 - 4k_3\text{CosIntegral}[\pi] + (k_3 - 1)\text{CosIntegral}[2\pi] + \log[2\pi] + k_3\log\left[\frac{\pi^3}{2}\right]\Big) \tag{12}$$

In Figure 3, we plot μ_{min} for different anisotropies of Frank elastic constants. One sees that for reasonable values of K_{24} the DT periodicity monotonically increases upon increasing K_{24}.

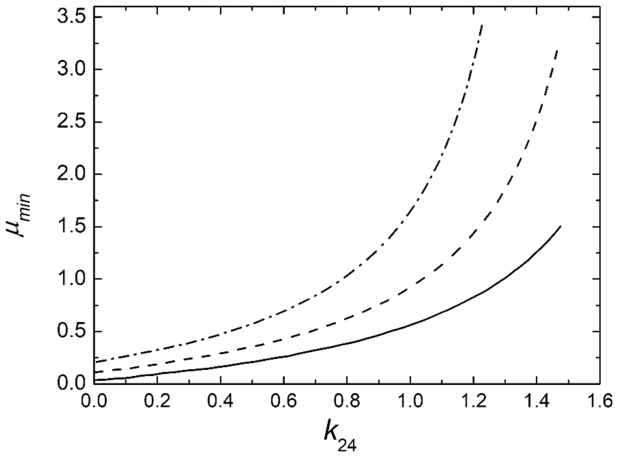

Figure 3. $\mu_{min} = Q_{min}/q$ as a function of $k_{24} = K_{24}/K_{22}$ for different values of $k_3 = K_{33}/K_{22}$. Full line, $k_3 = 1$; dashed line, $k_3 = 2$; dashed-dotted line, $k_3 = 3$.

Next, we illustrate how a simple Landau-type analysis reveals conditions promoting DT-like local excitations. We introduce scaled dimensionless periodicities

$$Q_0 = q_0 R,\ Q_{DT} = QR \tag{13}$$

and integrate the free energy density given by eq 10 in the cylindrical volume of the height h and radius R and expand the resulting free energy expression ΔF_{DT} in powers of Q_{DT}. Therefore, we consider examples satisfying the condition $QR < 1$ (e.g., $QR \sim \pi/4$ in the so-called half skyrmions realized in conventional blue phases[46]). Landau expansion yields

$$\frac{\Delta F_{DT}}{2\pi h K_{22}} = (1 - k_{24})Q_{DT}^2 + \frac{1}{24}(-8 + 8k_{24} + 3k_3)Q_{DT}^4 - k_2 Q_{DT} Q_0 + \frac{1}{6}k_2 Q_{DT}^3 Q_0 + F_0 \tag{14}$$

where F_0 is independent of Q_{DT}. In achiral samples, it follows

https://doi.org/10.1021/acsomega.2c07174
ACS Omega 2023, 8, 169−179

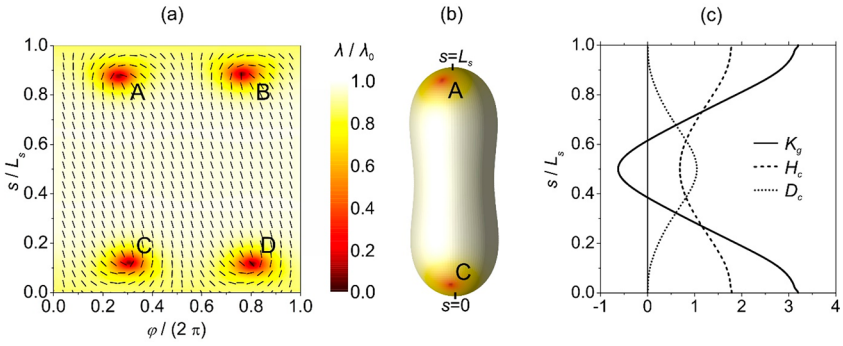

Figure 4. Order parameter profiles of equilibrium prolate nematic shell shape. (a) The nematic director field is superimposed onto the order parameter profile λ/λ_0 in the φ/s plane (λ_0 describes the bulk equilibrium value of λ). (b) 3D shell shape. (c) Gaussian curvature (K_g), mean curvature (H_c), and deviatoric curvature (D_c) of the shape. $\nu = 0.80$, $R/\xi = 7$, $k = \kappa$. Positions of TDs are marked with capital letters. $R = \sqrt{A/4\pi}$.

$$\frac{\Delta F_{DT}}{2\pi h K_{22}} = (1 - k_{24})Q_{DT}^2 + \frac{1}{24}(-8 + 8k_{24} + 3k_3)Q_{DT}^4 + F_0 \quad (15)$$

Therefore, the double-twist excitation could be stabilized only for $k_{24} > 1$, which is not realized in conventional LCs due to the Ericksen stability condition,[47] which limits the maximal value of K_{24}.

On the contrary, in chiral samples, the DT excitations are always (meta) stable. Minimization of ΔF_{DT} taking into account the expansion up to the quadratic term in Q_{DT} yields

$$Q = \frac{q_0}{2(1 - K_{24}/K_{22})} \quad (16)$$

and

$$\frac{\Delta F_{DT}}{2\pi h K_{22}} = -\frac{k_{24}Q_0^2}{4(1 - k_{24})} \quad (17)$$

Note that $\Delta F_{DT} < 0$ for $k_{24} < 1$.

We next discuss the stability of the Meron[46]-type structure, which could be observed in thin films. Merons are determined by DT cylinders for which QR = $\pi/2$. They can form periodic structures which are enabled by a lattice of line disclinations $m = -1/2$ running along the cylinder axis as depicted in Figure 2c. Their presence is required topologically. Note that the central regions of DTs correspond to nonsingular 3D patterns, characterized by $m = 1$ winding number in the x/y plane. This structure avoids singularity via local escape of the nematic director field along the z axis. The total LC structure is topologically neutral (i.e., the total 3D charge and 2D charge in each plane equal to zero). Consequently, within the x/y plane, each DT's imposed $m = 1$ "escaped" singularity must be compensated by two $m = -1/2$ disclinations.

Further pieces of evidence that suggest the stability of the separated local assembly of $\{-1/2, 1, -1/2\}$ TDs results from the analysis of the saddle-splay elasticity within the Meron structure. The related free energy density contribution can be expressed as $f_{24} = -2K_{24}K_G$ (see eq 6). The Meron-type excitation exhibits regions displaying $K_G > 0$ (the central "escaped" volume) and $K_G < 0$ (the outer part). 2D studies suggest[48] that regions exhibiting $K_G > 0$ ($K_G < 0$) attract defects with $m > 0$ ($m < 0$). Therefore, if a Meron-like excitation is formed in the nematic fluid, one expects that regions exhibiting $K_G > 0$ ($K_G < 0$) attract $m > 0$ ($m < 0$) defects. In addition, the saddle-splay elasticity locally renormalizes temperature. To illustrate this, we focus on the quadratic condensation term and the saddle-splay elastic term (we label them as f_2) close to the $I-N$ phase transition, where quadratic terms in S dominate. Taking into account[8] $K_{24} \sim LS^2$, it follows that $f_2 = a_0(T - T^*)S^2 - 2K_{24}K_G = a_0(T - T^*_{eff})S^2$, where

$$T^*_{eff} = T^* + \frac{2L}{a_0}K_G \quad (18)$$

Note that in the absence of other elastic contributions, the resulting phase transition temperature reads $T_c = T^*_{eff} + \frac{b^2}{4a_0c}$. Therefore, LC regions exhibiting $K_G > 0$ ($K_G < 0$) exhibit effectively lower (higher) temperatures. Consequently, regions with $K_G > 0$ promote orientational order and consequently unsplit $m = 1$ local structure escaping[49] along the third dimension. On the other hand, in $K_G < 0$ regions, singular $m = -1/2$ structures are preferred.

3.2. Curvature Driven Stabilization. The impact of curvature on TDs is well explored in 2D curved manifolds exhibiting in-plane ordering. Most studies[48,50−53] have been based on XY-type modeling. Note that there are several experimental systems where such predictions could be realized. Examples include biological membranes[54] and LC shells.[51,52,55−57] Theoretical studies and simulations reveal that surface patches possessing $K_G > 0$ and $K_G < 0$ are an attractor for point TDs bearing $m > 0$ and $m < 0$, respectively. This could be intuitively guessed by considering the Gauss−Bonnet and Poincare−Hopf theorems.[58] According to them, the total winding number m_{tot} of TDs hosted by the ordering field on a closed surface equals

$$m_{tot} = \chi = \frac{1}{2\pi}\oint K_G\, dA \quad (19)$$

Here, dA stands for the infinitesimally small surface patch, $\chi = 2(1 - g)$ is the Euler characteristic of the closed surface, and the genus g counts the number of the holes that the surface exhibits. For example, for spherical topology, it holds $g = 0$ and $m_{tot} = 2$. The differential form of eq 19 suggests

$$dm_{tot} = \frac{dA}{2\pi}K_G \quad (20)$$

Therefore, $K_G > 0$ ($K_G < 0$) locally enforces $dm_{tot} > 0$ ($dm_{tot} > 0$). According to the Effective Topological Charge Cancellation[59] (ETCC) mechanism, each surface patch, to which one assigns a characteristic spatially average value of K_G, tends to

https://doi.org/10.1021/acsomega.2c07174
ACS Omega 2023, 8, 169−179

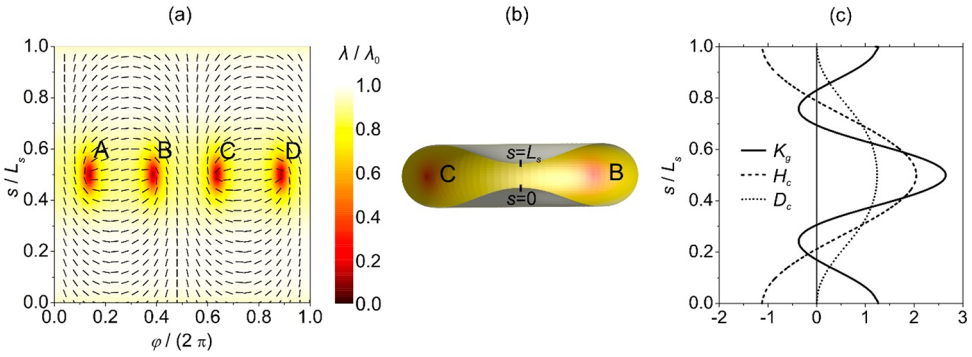

Figure 5. Order parameter profiles of equilibrium oblate nematic shell shape. (a) The nematic director field is superimposed onto the order parameter profile λ/λ_0 in the φ/s plane. (b) 3D shell shape. (c) Gaussian curvature (K_g), mean curvature (H_c), and deviatoric curvature (D_c) of the shape. $v = 0.60$, $R/\xi = 7$, $k = \kappa$. Positions of TDs are marked with capital letters.

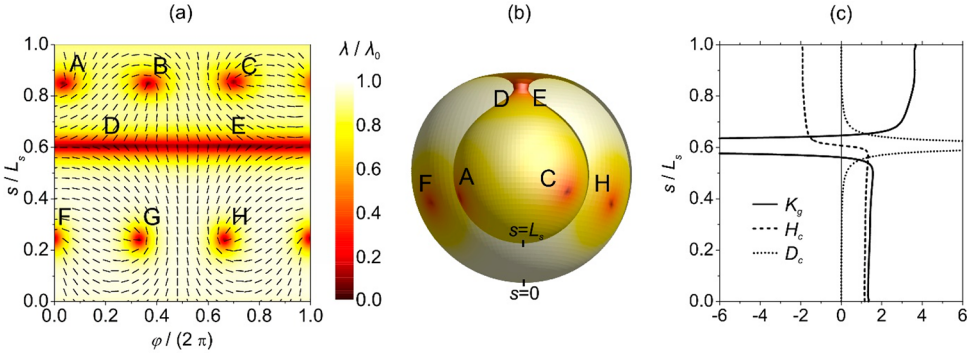

Figure 6. Order parameter profiles of equilibrium stomatocyte nematic shell shape. (a) The nematic director field is superimposed onto the order parameter profile λ/λ_0 in the φ/s plane. (b) 3D shell shape. (c) Gaussian curvature (K_g), mean curvature (H_c), and deviatoric curvature (D_c) of the shape. $v = 0.20$, $R/\xi = 7$, $k = \kappa$. Positions of TDs are marked with capital letters.

be *topologically neutral*. Therefore, the "smeared Gaussian curvature charge" (the right-hand of eq 20) is screened by winding number or "real" (the left-hand of eq 20). This local tendency can be realized by rearranging existing TDs or by creating additional pairs {*defect*, *antidefect*}. The latter process is possible if regions exhibiting strong enough local curvatures are present.

To illustrate this curvature driven assembling of TDs, we consider closed surfaces (shells) of revolution exhibiting in-plane nematic order. The corresponding 2D Landau–de Gennes–Helfrich model[54] is summarized in the Appendix. The orientational order is presented by in-plane nematic director field **n** and 2D order parameter field λ, which equals zero exactly at the center of a point defect. The relationship between 3D and 2D tensor nematic order parameters is described in ref 60. In modeling, we change the shape of shells and calculate the related nematic texture. The shape is determined by a relative volume $v = \frac{V}{V_0} \in [0, 1]$ of a shell. Here, V refers to the volume enclosed by an axially symmetric shape of total surface area A, and V_0 is the volume of the sphere having the same surface area.

In Figures 4–6, we plot a characteristic pattern of defects in different shell geometries which all exhibit spherical topology which imposes $m_{tot} = 2$. Consequently, in a large enough spherical shell (i.e., its radius is much larger than the nematic order parameter correlation length), such a structure would exhibit four $m = 1/2$ defects. These defects are mutually repelling and in a spherical shell occupy corners of a hypothetical tetrahedron[52,57] inscribed within the sphere. In prolate shells (Figures 4), which are stable for relatively large values of v, these TDs are shifted toward the poles of a shape. Namely, at its poles, the Gaussian curvature exhibits a maximal positive value, and consequently the poles represent attractors for TDs bearing $m > 0$. The position of defects reveals the compromise between the attraction of $m = 1/2$ defects to the poles and their mutual repulsion. In the regime of intermediate values[54] of the relative volume, disk-like shapes are established, see Figure 5. This geometry exhibits maximal Gaussian curvature at the equatorial line. Consequently, the four mutually repelling TDs are assembled along this line. Finally, for relatively low values of v, the so-called stomatocyte shapes are formed, see Figures.6. In these structures, neck-like regions exhibiting relatively large values of $|K_g|$ exist, which enable local formation of an additional two {*defect*, *antidefect*}. The two $m = -1/2$ *antidefects* are assembled within the neck where $K_g < 0$. The remaining six mutually repelling $m = 1/2$ defects are assembled in regions where $K_g > 0$.

3.3. Phase Transition and Disorder Driven Stabilization of TDs. The most ubiquitous source of TDs is fast enough symmetry breaking phase transitions, which is explained by the universal Kibble–Zurek mechanism.[1,61] Note that the mechanism was originally introduced in cosmology to model coarsening dynamics of topological defects in the Higgs field in the early universe. The only two conditions that need to be fulfilled for the KZ mechanism are continuous symmetry breaking and a finite velocity of information propagation. According to it, the following features are expected. If a phase change is realized on a short enough time scale with respect to the relevant amplitude order

https://doi.org/10.1021/acsomega.2c07174
ACS Omega 2023, 8, 169–179

parameter relaxation time, then order in well-enough separated spatial regions is not correlated due to the finite speed of information propagation. Consequently, different symmetry breaking directions are in general selected. Domains are formed, within which the *phase* ordering field points along a similar direction. At domain interfaces, topological defects are created.

The subsequent domain growth is enabled by the annihilation of *defects* and *antidefects*. This reduces the concentration of energetically expensive domain walls. In common cases and in the absence of "impurities," the characteristic linear size of domains grows with time, exhibiting a universal scaling law[62,63] $\xi_d \propto t^{\gamma}$, where γ is the scaling coefficient. Note that qualitatively different TDs appear for polar and axial (i.e., quadrupole) symmetry breaking fields. The former can exhibit topologically stable point defects. On the contrary, nematic-like order also allows line defects.

The presence of "impurities", which often act effectively as random-field like disorder, can arrest the domain growth and consequently stabilize TDs. In particular, phases reached by continuous symmetry-breaking phase transition are particularly susceptible to disorder due to the existence of easily excitable Goldstone modes. According to the Imry−Ma theorem,[64] even an infinitesimally weak random-field type of disorder can destroy long-range order of a pure system. The resulting structure is expected to exhibit short-range order, characterized by the Imry−Ma domain size $\xi_d^{(\mathrm{IM})} \propto w^{-2/(4-d)}$. Here, w measures the disorder strength and d stands for the spatial dimensionality. However, several studies reveal[65−68] that, for weak enough disorder, quasi-long-range order or even long-range order might be established.

In the following, we illustrate the derivation of the characteristic size $\xi_d^{(\mathrm{p})}$ of protodomains that are nucleated via the universal Kibble−Zurek (KZ) mechanism. We show that created domains could significantly depress the resulting phase transition temperature, which has not yet been reported. As a demonstrating example, let us consider a fast enough isotropic−nematic phase transition. Let us describe the temperature variation by the dimensionless temperature $r = (T - T^*)/T^*$, where T^* stands for the supercooling temperature. Namely, in a fast enough isotropic phase, supercooling is very likely. We characterize the fast quench by linear time dependence characterized by the quench rate τ_Q:

$$t = -\tau_Q r \tag{21}$$

Here, τ_Q describes the time needed to increase the temperature from $T = 0$ to T^*. Close to weakly first-order $I-N$ phase transition, the characteristic amplitude order parameter relaxation length and relaxation time obey equations

$$\tau \approx \frac{\tau_0}{|r|^{\eta}},\ \xi \approx \frac{\xi_0}{|r|^{\nu}} \tag{22}$$

τ_0 and ξ_0 determine characteristic responses deep in the symmetry broken phase, and in typical nematic LC it holds $\eta \sim 1$ and $\nu \sim 1/2$. These values of critical exponents are also predicted by the mean-field description.

To estimate the size of first formed domains, the so-called *protodomains* of size ξ_p, one originates from the disordered phase. The maximal size of fluctuations exhibiting locally (para) nematic order within the disordered isotropic "sea" is estimated by ξ (see eq 22). The temperature regime where $|t| > \tau$ is referred to as the "impulse" regime. In it, the dynamic of the system is fast enough to adapt to changes in temperature, and the system displays a roughly equilibrium-like order. The qualitative change in behavior is expected when the time to reach the phase transition becomes comparable to the relaxation time. This time is termed as the Zurek time and is defined by the condition $|t_z| = \tau$. It follows

$$|t_z| \sim (\tau_0 \tau_Q^{\eta})^{1/1+\eta} \sim \sqrt{\tau_0 \tau_Q} \tag{23}$$

In the so-called adiabatic time regime $-|t_z| < t < |t_z|$, the order parameter dynamics are relatively slow. In approximate treatment, one assumes that the dynamics are frozen in and the system falls out of equilibrium. When the system exits the adiabatic regime at $t = |t_z|$, the dynamics unfreeze. The size of the largest fluctuation generated clusters in the isotropic phase, which "survive" the phase adiabatic time regime crossing, is estimated by

$$\xi^{(\max)} = \xi\left(|r_z| = \frac{|t_z|}{\tau_Q}\right)\xi_0\left(\frac{\tau_Q}{\tau_0}\right)^{\nu/1+\eta} \sim \xi_0\left(\frac{\tau_Q}{\tau_0}\right)^{1/4} \tag{24}$$

and $\xi_p \sim \xi^{(\max)}$.

We suggest that the elastic free energy contribution should also be included in the analysis, which was neglected in the original estimates made by Zurek. Below, we present expected related consequences which could be experimentally tested.

We express the free energy density as $f \sim f_c + f_e$, where (see eq 3)

$$f_c \approx a_0(T - T^*)S^2 - bS^3 + cS^4 \tag{25a}$$

$$f_e \approx LS^2|\nabla \mathbf{n}|^2 + L|\nabla S|^2 \tag{25b}$$

We thus neglect biaxial states. We assume that the quench is realized fast enough so that domain structure in the director field is established after the Zurek time. With this in mind, we set $|\nabla \mathbf{n}|^2 \approx 1/\xi_d^2$, where ξ_d describes a typical domain size. As a reminder, the director relaxation is slower than that of S. It follows that

$$\begin{aligned} f_c &\approx a_0(T - T^*)S^2 - bS^3 + cS^4 + \frac{LS^2}{\xi_d^2} \\ &= a_0(T - T_{\mathrm{eff}}^*)S^2 - bS^3 + cS^4 \end{aligned} \tag{26}$$

where $T_{\mathrm{eff}}^* = T^*\left(1 + \frac{L}{a_0 T^* \xi_d^2}\right) \approx T^*\left(1 + \frac{\xi_0^2}{\xi_d^2}\right)$. Note that in bulk equilibrium it holds that $T_{\mathrm{IN}} = T^* + b^2/(4a_0 b)$. Therefore, the elastic distortions effectively decrease the local phase transition temperature:

$$T_{\mathrm{IN}}^{(\mathrm{eff})} = T_{\mathrm{IN}} - T^*\frac{\xi_0^2}{\xi_d^2} \tag{27}$$

For example, for the 5CB LCs request, $\Delta T_{\mathrm{IN}} = |T_{\mathrm{IN}} - T_{\mathrm{IN}}^{(\mathrm{eff})}| \approx 1K$ would suggest that $\xi_d \approx \xi_0\sqrt{T^*/\Delta T_{\mathrm{IN}}} \approx 52$ nm, which is a sensible value.

4. DISCUSSION

In most familiar examples, TDs in nematic LCs are stabilized by appropriate boundary conditions at LC-confining body interfaces.[10,14,30,34,38,39] In these cases, surface conditions impose topological constraints (embodied in nonzero topological charges) that stabilize various configurations of TDs. Within a region, the total topological charge q_{tot} (i.e., m_{tot} in 2D) is determined by topologically imposed constraints. Note

https://doi.org/10.1021/acsomega.2c07174
ACS Omega 2023, 8, 169−179

that for a given value of q_{tot} there can be different configurations of defects, which however must obey the topological charge conservation law. Therefore, for instance, strong thermal fluctuations could trigger a transformation between two different competing structures hosting TDs; however, q_{tot} remains unchanged.

In the present paper, we consider first cases where the total topological charge of the system equals zero. In such a setting, TDs are not enforced topologically but can be stabilized on energy grounds. For illustration, we use a simple Landau-type analysis. It reveals conditions that set fertile ground to form TDs. We demonstrate that a combination of chirality and saddle-splay elasticity may promote strong enough double-twist fluctuations. The latter might stabilize localized phase field distortions which are in a relevant 2D cross-section characterized by winding numbers $\{-1/2, 1, -1/2\}$. Such an assembly is topologically neutral and could be embedded in a uniform director far-field. Furthermore, the resulting saddle-splay deformation changes local effective temperature. For $K_{24} > 0$ (which is commonly realized[8] in nematic LCs), the local director field exhibits a positive Gaussian curvature K_g profile which effectively decreases local temperature. Consequently, this region favors the escaped nonsingular $m = 1$ deformation, which does not require local LC melting. On the contrary, regions possessing $K_g < 0$ (and a concomitant local increase in T) are more favorable for $m = -1/2$ distortions whose cores require a local change of LC amplitude. Such assemblies are in LCs referred to as merons.[46] In confined geometries,[16,24] merons could be stable even as isolated entities, where their structure could be studied using relatively simple confocal polarizing microscopy.[16] Furthermore, in such a setting, their structure could be enlarged, i.e., making it even better experimentally approachable, by approaching the critical point.[69] Namely, close to critical points, relevant order parameter amplitude correlation time and correlation length diverge.[8] One could tune critical conditions[70−73] simply by reducing the cell thickness, supposing that the surface-wetting interaction has a term that is linearly conjugated with the order parameter amplitude. Note that merons are members of the skyrmion family,[46] which has several analogs[6,74] in other branches of physics. Experiments in LCs evidence that strong enough chirality allows stabilization of quarter skyrmions, half skyrmions, or structures between the mentioned two configurations.[75] Indeed, skyrmions (the so-called full-skyrmions) were first introduced in particle physics to explain the structure of mesons and baryons.[6] Therefore, LCs provide a particularly convenient testbed to study in detail the fundamental properties of such localized structures.

The importance of K_g in stabilizing TDs is evidently shown in 2D structure via Gauss−Bonnet and Hopf−Poincare theorems.[58] Note that these theorems are based on universal parallel transport.[76−79] It was originally introduced to describe parallel lines in curved manifolds.[76,79,80] Based on that, general relativistic theory was developed in which the curvature of space−time emerges as a gravitational force. Parallel transport was also used in nematic LCs to determine the presence of defects[57,81,82] (i.e., regions exhibiting nonzero winding number) in a given surface patch hosting nematic order. Furthermore, using it, one can define intrinsic and extrinsic geometric potentials[82] which determine regimes where defects are likely to appear without solving Euler−Lagrange equations. Extremes of the intrinsic geometric potential are in general attracting TDs. On the contrary, regions exhibiting a large absolute value of the extrinsic geometric potential repel TDs. To calculate the potentials, one essentially needs only information about the geometry[54] of the manifold which hosts nematic order. These and other studies reveal that nematic LCs are perfectly suited to study the impact of curvature on TDs. Furthermore, concepts developed in 2D, where phenomena could be relatively visualized, could be applied to higher manifolds exhibiting higher dimensionalities.[58]

Efficient generators of TDs are also sudden changes in systems. Due to them, distant enough regions cannot synchronize their ordering. Resulting frustrations are often resolved by the creation of TDs. Consequently, in fast enough symmetry phase transition domains are formed. Note that the early $I-N$ coarsening dynamic is dominated by chargeless (twist) disclination loops.[32] Therefore, these TDs are most ubiquitous in the early regime. They weakly interact with the surrounding nematic structure, and they gradually vanish because they are not topologically protected.[83,84] Recent studies[39,85] suggest that these disclinations can act simultaneously like *defects* and *antidefects*. This remains somehow for Majorna particles[86] and neutrinos, the behaviors of which are still not fundamentally understood. Note that recent experimental[18,41,87] studies suggest that twist nematic loops could be stabilized by toroidal topology. In these studies, colloids of toroidal topology, where their surface enforces homeotropic anchoring (i.e., nematic director tends to be aligned along the local surface normal), are immersed in nematic LC. Note that in 3D the torus does not enforce the 3D topological charge.[41] However, 2D analysis reveals that TDs must be present. Therefore, either pair or pairs {*defect,antidefect*} are formed, or chargeless loops. Namely, a torus possesses regions exhibiting $K_g > 0$ and $K_g < 0$, which individually attract different signs of winding number. Recent experiments[87] reveal that torus geometry efficiently stabilizes twist loops in chiral LCs. Hence, if neutrinos have roughly similar local structures, they could be stabilized by an appropriate topology of higher dimensional space (exhibiting alternating $K_g > 0$ and $K_g < 0$ regions) in the string theory description of nature.

Finally, if impurities are present, they could stabilize[88,89] TDs which are formed in a fast enough quench. The resulting phase might exhibit glass behavior,[89,90] which also represents an open problem in physics. Therefore, looking at the glass problem from the perspective of curvature-trapped TDs might yield some additional understanding in the field.

5. CONCLUSIONS

TDs in a physical field are inevitably formed in symmetry-breaking phase transitions. Such transitions allow the existence of competing configurations whose coexistence is enabled by TDs. Namely, their local structure permits realization of large changes in ordering on relatively short length scales, and for this reason they serve as mediators between "conflicting" regions. There are several pieces of evidence that curvature plays a crucial role in stabilizing TDs. An ideal testing bed to study curvature-driven stabilization of TDs is thermotropic nematic LCs. They exhibit temperature-driven isotropic−nematic phase transition in which continuous rotational symmetry is broken. Established orientational order is commonly described by the second rank traceless and symmetric tensor nematic order parameter, which is in bulk equilibrium determined by scalar order parameter (amplitude)

https://doi.org/10.1021/acsomega.2c07174
ACS Omega 2023, 8, 169−179

field and nematic director (phase) field. The equilibrium degeneracy of the latter enables the existence of TDs. We have illustrated using a simple Landau-type analysis how the combining effect of chirality and saddle splay elasticity could stabilize TDs in a system whose total topological charge equals zero. In this case, TDs are stabilized due to inherent "defect-fertile" conditions within the system. The saddle-splay deformation is in turn related to the Gaussian curvature of hypothetical planes whose normal is pointing along local nematic director field **n**. In general, the impact of Gaussian curvature and curvature on TDs is well explored in 2D systems, and we have provided typical examples which manifest these effects. Furthermore, curvature in **n** patterns could be nucleated in a fast enough phase transion, and generated TDs could be stabilized by impurities present in the system. Similar phenomena are expected to appear in other systems reached via continuous symmetry-breaking phase transitions.

APPENDIX: 2D LANDAU–DE GENNES–HELFRICH MESOSCOPIC APPROACH

The geometry of the shape, whose local normal is given by **v**, is determined by the curvature tensor[90,91] **C**, and the orientational ordering on the shape is described by the 2D nematic tensor order parameter[81] $\mathbf{Q}^{(2D)}$. These tensors are expressed in their eigenframes as

$$\mathbf{C} = C_1\mathbf{e}_1 \otimes \mathbf{e}_1 + C_2\mathbf{e}_2 \otimes \mathbf{e}_2 \tag{A1}$$

$$\mathbf{Q}^{(2D)} = \lambda(\mathbf{n} \otimes \mathbf{n} - \mathbf{n}_\perp \otimes \mathbf{n}_\perp) \tag{A2}$$

In eq A1, the unit vectors $\{\mathbf{e}_1,\mathbf{e}_2\}$ determine a local principal curvature frame, where $\{C_1,C_2\}$ are the corresponding principal curvatures. In eq A2, the nematic director fields **n** and $\mathbf{n}_\perp$ correspond to the $\mathbf{Q}^{(2D)}$ eigenvectors, where $\mathbf{v} = \mathbf{n} \times \mathbf{n}_\perp$, and $\lambda \in [0, 1/2]$ is the orientational order parameter. The free energy contributions $f = f_H + f_c + f_e$ are expressed as follows:

$$f_H = \frac{\kappa}{2}(Tr\ \mathbf{C})^2 \tag{A3}$$

$$f_c = \alpha_0(T - T_c)Tr\ \mathbf{Q}^{(2D)^2} + \frac{\beta}{4}(Tr\ \mathbf{Q}^{(2D)^2})^2 \tag{A4}$$

$$f_e = \frac{1}{2}k|\nabla_s\mathbf{Q}^{(2D)}|^2 \tag{A5}$$

where f_H stands for the classical Helfrich contribution,[90] which resists surface bending deformations for a positive bending modulus κ. The nematic condensation contribution f_c is enforcing equilibrium nematic orientational order $\lambda_0 = \sqrt{\alpha_0(T_c - T)/\beta}$ below a critical temperature T_c. The quantities α_0 and β are positive phenomenological constants. The elastic contribution f_e is weighted by the positive elastic constant k; ∇_s stands for the surface gradient operator.[81]

In simulations, we restrict to closed axisymmetric two-dimensional shells exhibiting spherical topology. The shell surface is constructed by the rotation of the profile curve about the z axis by an angle of $\varphi = 2\pi$ in order to obtain a surface of revolution. A generic point on the surface is given by[59]

$$\mathbf{r} = \rho(s)\cos\varphi\mathbf{e}_x + \rho(s)\sin\varphi\mathbf{e}_y + z(s)\mathbf{e}_z \tag{A6}$$

where $\rho(s)$ and $z(s)$ are the coordinates of the profile in the ρ/z plane and s represents the arc length of the profile curve. The total length of the arc of a profile is denoted by L_s. We define that the principal directions ($\mathbf{e}_1$, $\mathbf{e}_2$; see eq A1) point along meridians (φ = *const*) and parallels (s = *const*), since these are the lines of principal curvatures $\{C_1,C_2\}$. On any point on the surface, we can calculate the Gaussian curvature $K_g = C_1\ C_2$, the mean curvature $H_c = \frac{1}{2}(C_1 + C_2)$, and the deviatoric curvature $D_c = \frac{1}{2}|C_1 - C_2|$.

AUTHOR INFORMATION

Corresponding Author

Samo Kralj − *Faculty of Natural Sciences and Mathematics, University of Maribor, 2000 Maribor, Slovenia; Jožef Stefan Institute, 1000 Ljubljana, Slovenia;* orcid.org/0000-0002-3962-8845; Email: samo.kralj@um.si

Authors

Arbresha Hölbl − *Faculty of Natural Sciences and Mathematics, University of Maribor, 2000 Maribor, Slovenia*

Luka Mesarec − *Faculty of Electrical Engineering, University of Ljubljana, 1000 Ljubljana, Slovenia*

Juš Polanšek − *Faculty of Natural Sciences and Mathematics, University of Maribor, 2000 Maribor, Slovenia*

Aleš Iglič − *Faculty of Electrical Engineering, University of Ljubljana, 1000 Ljubljana, Slovenia*

Complete contact information is available at: https://pubs.acs.org/10.1021/acsomega.2c07174

Author Contributions

S.K. initiated this study. S.K. and A.H. wrote the manuscript. L.M. and A.I. developed a Monte Carlo program for the calculation of nematic profiles, and L.M. performed the numerical simulations. A.H. and J.P. developed the Landau approach in studying merons and prepared the figures.

Notes

The authors declare no competing financial interest.

ACKNOWLEDGMENTS

The authors acknowledge support from the Slovenian Research Agency grants P1-0099, J1-2457, and J2-4447.

REFERENCES

(1) Zurek, W.-H. Cosmological experiments in superfluid helium? *Nature* **1985**, *317*, 505−508.

(2) Sethna, J.-P. Order parameters, broken symmetry, and topology. *arXiv preprint* **1992**, cond-mat/9204009.

(3) Chaikin, P.-M.; Lubensky, T.-C.; Witten, T.-A. *Principles of Condensed Matter Physics*; Cambridge University Press: Cambridge, 1995.

(4) Hobson, A. There are no particles, there are only fields. *Am. J. Phys.* **2013**, *81*, 211−223.

(5) Ball, R.-D.; Candido, A.; Cruz-Martinez, J.; Forte, S.; Giani, T.; Hekhorn, F.; Kudashkin, K.; Magni, G.; Rojo, J. Evidence for intrinsic charm quarks in the proton. *Nature* **2022**, *608*, 483−487.

(6) Skyrme, T.-H.-R. A unified field theory of mesons and baryons. *Nucl. Phys.* **1962**, *31*, 556−569.

(7) Duda, J. Framework for liquid crystal based particle models. *arXiv preprint*, **2021**, arXiv:2108.07896.

(8) Kleman, M.; Lavrentovich, O.-D. *Soft Matter Physics: An Introduction*; Springer: New York, 2003; pp 337−387.

(9) Mermin, N.-D. The topological theory of defects in ordered media. *Rev. Mod. Phys.* **1979**, *51*, 591.

(10) Kurik, M.-V.; Lavrentovich, O.-D. Defects in liquid crystals: homotopy theory and experimental studies. *Sov. Phys. Usp.* **1988**, *31*, 196.

(11) Oswald, P.; Pieranski, P. *Liquid Crystals: Concepts and Physical Properties Illustrated by Experiments*, 1st ed.; CRC Press, 2018.

https://doi.org/10.1021/acsomega.2c07174
ACS Omega 2023, 8, 169−179

(12) Gaeta, G.; Virga, E.-G. Octupolar order in three dimensions. *Eur. Phys. J. E* **2016**, *39*, 1−16.
(13) Machon, T.; Alexander, G.- P. Umbilic lines in orientational order. *Phys. Rev. X* **2016**, *6*, 011033.
(14) Volovik, G.-E.; Lavrentovich, O.-D. Topological dynamics of defects: boojums in nematic drops. *Zh. Eksp. Teor. Fiz.* **1983**, *85*, 1997−2010.
(15) Chuang, I.; Durrer, R.; Turok, N.; Yurke, B. Cosmology in the laboratory: Defect dynamics in liquid crystals. *Science* **1991**, *251*, 1336−1342.
(16) Nych, A.; Fukuda, J.-I.; Ognysta, U.; Žumer, S.; Muševič, I. Spontaneous formation and dynamics of half-skyrmions in a chiral liquid-crystal film. *Nat. Phys.* **2017**, *13*, 1215−1220.
(17) Smalyukh, I.-I.; Lansac, Y.; Clark, N.-A.; Trivedi, R.-P. Three-dimensional structure and multistable optical switching of triple-twisted particle-like excitations in anisotropic fluids. *Nat. Mater.* **2010**, *9*, 139−145.
(18) Smalyukh, I.-I. Knots and other new topological effects in liquid crystals and colloids. *Rep. Prog. Phys.* **2020**, *83*, 106601.
(19) Poulin, P.; Stark, H.; Lubensky, T.-C.; Weitz, D.-A. Novel colloidal interactions in anisotropic fluids. *Science* **1997**, *275*, 1770−1773.
(20) Tkalec, U.; Ravnik, M.; Čopar, S.; Žumer, S.; Muševič, I. Reconfigurable knots and links in chiral nematic colloids. *Science* **2011**, *333*, 62−65.
(21) De Gennes, P.-G. An analogy between superconductors and smectics A. *Solid State Commun.* **1972**, *10*, 753−756.
(22) Lubensky, T.-C.; Renn, S.-R. Twist-grain-boundary phases near the nematic−smectic-A−smectic-C point in liquid crystals. *Phys. Rev. A* **1990**, *41*, 4392.
(23) Bradač, Z.; Kralj, S.; Žumer, S. Early stage domain coarsening of the isotropic-nematic phase transition. *J. Chem. Phys.* **2011**, *135*, 024506.
(24) Fukuda, J.-I.; Žumer, S. Quasi-two-dimensional Skyrmion lattices in a chiral nematic liquid crystal. *Nat. Commun.* **2011**, *2*, 1−5.
(25) Ravnik, M.; Žumer, S. Landau−de Gennes modelling of nematic liquid crystal colloids. *Liq. Cryst.* **2009**, *36*, 1201−1214.
(26) Selinger, J.-V. Interpretation of saddle-splay and the Oseen-Frank free energy in liquid crystals. *Liq. Cryst. Rev.* **2018**, *6*, 129−142.
(27) Selinger, J.-V. Director deformations, geometric frustration, and modulated phases in liquid crystals. *Annu. Rev. Condens. Matter Phys.* **2022**, *13*, 49−71.
(28) Meiboom, S.; Sethna, J.-P.; Anderson, P.-W.; Brinkman, W.-F. Theory of the blue phase of cholesteric liquid crystals. *Phys. Rev. Lett.* **1981**, *46*, 1216.
(29) Svenšek, D.; Žumer, S. Instability modes of high-strength disclinations in nematics. *Phys. Rev. E* **2004**, *70*, 061707.
(30) Kralj, S.; Murray, B.-S.; Rosenblatt, C. Decomposition of strongly charged topological defects. *Phys. Rev. E* **2017**, *95*, 042702.
(31) Kosterlitz, J.-M.; Thouless, D.-J. Ordering, metastability and phase transitions in two-dimensional systems. *J. Phys. C: Solid State Phys.* **1973**, *6*, 1181.
(32) Billeter, J.-L.; Smondyrev, A.-M.; Loriot, G.-B.; Pelcovits, R.-A. Phase-ordering dynamics of the Gay-Berne nematic liquid crystal. *Phys. Rev. E* **1999**, *60*, 6831−6840.
(33) Lavrentovich, O.-D.; Terent'ev, E.-M. Phase transition altering the symmetry of topological point defects (hedgehogs) in a nematic liquid crystal. *Zh. Eksp. Teor. Fiz.* **1986**, *91*, 2084−2096.
(34) Lavrentovich, O.-D.; Ishikawa, T.; Terentjev, E.-M. Disclination loop in Mori-Nakanishi ansatz: role of the divergence elasticity. *Mol. Cryst. Liq. Cryst. Sci. Technol. Section A. Mol. Cryst. Liq. Cryst.* **1997**, *299*, 301−306.
(35) Kralj, S.; Virga, E.-G.; Žumer, S. Biaxial torus around nematic point defects. *Phys. Rev. E* **1999**, *60*, 1858−1866.
(36) Wang, X.; Miller, D.-S.; Bukusoglu, E.; De Pablo, J.-J.; Abbott, N.-L. Topological defects in liquid crystals as templates for molecular self-assembly. *Nat. Mater.* **2016**, *15*, 106−112.
(37) Wang, X.; Kim, Y. K.; Bukusoglu, E.; Zhang, B.; Miller, D. S.; Abbott, N. L. Experimental insights into the nanostructure of the cores of topological defects in liquid crystals. *Phys. Rev. Lett.* **2016**, *116*, 147801.
(38) Murray, B.-S.; Pelcovits, R.-A.; Rosenblatt, C. Creating arbitrary arrays of two-dimensional topological defects. *Phys. Rev. E* **2014**, *90*, 052501.
(39) Harkai, S.; Murray, B.-S.; Rosenblatt, C.; Kralj, S. Electric field driven reconfigurable multistable topological defect patterns. *Phys. Rev. Res.* **2020**, *2*, 013176.
(40) Lavrentovich, O.-D. Topological defects in dispersed words and worlds around liquid crystals, or liquid crystal drops. *Liq. Cryst.* **1998**, *24*, 117−126.
(41) Senyuk, B.; Liu, Q.; He, S.; Kamien, R.-D.; Kusner, R.-B.; Lubensky, T.-C.; Smalyukh, I.-I. Topological colloids. *Nature* **2013**, *493*, 200−205.
(42) Palffy-Muhoray, P.; Gartland, E.-C.; Kelly, J.-R. A new configurational transition in inhomogeneous nematics. *Liq. Cryst.* **1994**, *16*, 713−718.
(43) Ambrožič, M.; Kralj, S.; Virga, E.-G. Defect-enhanced nematic surface order reconstruction. *Phys. Rev. E* **2007**, *75*, 031708.
(44) Schopohl, N.; Sluckin, T.-J. Defect core structure in nematic liquid crystals. *Phys. Rev. Lett.* **1987**, *59*, 2582−2584.
(45) Zhou, S.; Shiyanovskii, S.-V.; Park, H.-S.; Lavrentovich, O.-D. Fine structure of the topological defect cores studied for disclinations in lyotropic chromonic liquid crystals. *Nat. Commun.* **2017**, *8*, 1−7.
(46) Duzgun, A.; Selinger, J.-V.; Saxena, A. Comparing skyrmions and merons in chiral liquid crystals and magnets. *Phys. Rev. E* **2018**, *97*, 062706.
(47) Ericksen, J.-L. Inequalities in liquid crystal theory. *Phys. Fluids* **1966**, *9*, 1205−1207.
(48) Vitelli, V.; Turner, A.-M. Anomalous coupling between topological defects and curvature. *Phys. Rev. Lett.* **2004**, *93*, 215301.
(49) Cladis, P.-E.; Kleman, M. Non-singular disclinations of strength S = + 1 in nematics. *J. Phys. (Paris)* **1972**, *33*, 591−598.
(50) Bowick, M.; Nelson, D.-R.; Travesset, A. Curvature-induced defect unbinding in toroidal geometries. *Phys. Rev. E* **2004**, *69*, 041102.
(51) Nelson, D.-R. Toward a tetravalent chemistry of colloids. *Nano Lett.* **2002**, *2*, 1125−1129.
(52) Vitelli, V.; Nelson, D.-R. Nematic textures in spherical shells. *Phys. Rev. E* **2006**, *74*, 021711.
(53) Selinger, R.-L.-B.; Konya, A.; Travesset, A.; Selinger, J.-V. Monte Carlo studies of the XY model on two-dimensional curved surfaces. *J. Phys. Chem. B* **2011**, *115*, 13989−13993.
(54) Mesarec, L.; Góźdź, W.; Iglič, A.; Kralj-Iglič, V.; Virga, E.-G.; Kralj, S. Normal red blood cells' shape stabilized by membrane's in-plane ordering. *Sci. Rep.* **2019**, *9*, 1−11.
(55) Skačej, G.; Zannoni, C. Controlling surface defect valence in colloids. *Phys. Rev. Lett.* **2008**, *100*, 197802.
(56) Lopez-Leon, T.; Koning, V.; Devaiah, K.-B.-S.; Vitelli, V.; Fernandez-Nieves, A. Frustrated nematic order in spherical geometries. *Nat. Phys.* **2011**, *7*, 391−394.
(57) Rosso, R.; Virga, E.-G.; Kralj, S. Parallel transport and defects on nematic shells. *Contin. Mech. Thermodyn.* **2012**, *24*, 643−664.
(58) Kamien, R.-D. The geometry of soft materials: a primer. *Rev. Mod. Phys.* **2002**, *74*, 953.
(59) Mesarec, L.; Góźdź, W.; Iglič, A.; Kralj, S. Effective topological charge cancelation mechanism. *Sci. Rep.* **2016**, *6*, 27117.
(60) Kralj, S.; Majumdar, A. Order reconstruction patterns in nematic liquid crystal wells. *Proc. R. Soc. A: Math. Phys. Eng. Sci.* **2014**, *470*, 20140276.
(61) Kibble, T.-W.-B. Topology of cosmic domains and strings. *J. Phys. A: Math. Gen.* **1976**, *9*, 1387−1398.
(62) Bray, A. J. Theory of phase-ordering kinetics. *Adv. Phys.* **2002**, *51*, 481−587.
(63) Dierking, I. Universal growth laws in liquid crystals far from equilibrium. *Appl. Phys. A: Mater. Sci. Process.* **2001**, *72*, 307−310.
(64) Imry, Y.; Ma, S.-K. Random-field instability of the ordered state of continuous symmetry. *Phys. Rev. Lett.* **1975**, *35*, 1399−1401.

https://doi.org/10.1021/acsomega.2c07174
ACS Omega 2023, 8, 169−179

(65) Chakrabarti, J. Simulation evidence of critical behavior of isotropic-nematic phase transition in a porous medium. *Phys. Rev. Lett.* **1998**, *81*, 385.
(66) Feldman, D.-E. Quasi-long range order in glass states of impure liquid crystals, magnets, and superconductors. *Int. J. Mod. Phys. B* **2001**, *15*, 2945−2976.
(67) Giamarchi, T.; Le Doussal, P. Elastic theory of flux lattices in the presence of weak disorder. *Phys. Rev. B* **1995**, *52*, 1242−1270.
(68) Ranjkesh, A.; Ambrožič, M.; Kralj, S.; Sluckin, T.-J. Computational studies of history dependence in nematic liquid crystals in random environments. *Phys. Rev. E* **2014**, *89*, 022504.
(69) Lelidis, L.; Nobili, M.; Durand, G. Electric-field-induced change of the order parameter in a nematic liquid crystal. *Phys. Rev. E* **1993**, *48*, 3818.
(70) Sheng, P. Boundary-layer phase transition in nematic liquid crystals. *Phys. Rev. A* **1982**, *26*, 1610.
(71) Sluckin, T.-J.; Poniewierski, A. Novel surface phase transition in nematic liquid crystals: Wetting and the Kosterlitz-Thouless transition. *Phys. Rev. Lett.* **1985**, *55*, 2907.
(72) Sen, A. K.; Sullivan, D. E. Landau−de Gennes theory of wetting and orientational transitions at a nematic-liquid−substrate interface. *Phys. Rev. A* **1987**, *35*, 1391.
(73) Boamfa, M.-I.; Kim, M.-W.; Maan, J.-C.; Rasing, T. Observation of surface and bulk phase transitions in nematic liquid crystals. *Nature* **2003**, *421*, 149−152.
(74) Dierking, I.; Blenkhorn, W.; Credland, E.; Drake, W.; Kociuruba, R.; Kayser, B.; Michael, T. Stabilising liquid crystalline blue phases. *Soft Matter* **2012**, *8*, 4355−4362.
(75) Pišljar, J.; Ghosh, S.; Turlapati, S.; Rao, N.-V.-S.; Škarabot, M.; Mertelj, A.; Petelin, A.; Nych, A.; Marinčič, M.; Pusovnik, A.; Ravnik, M.; Muševič, I. Blue phase III: topological fluid of skyrmions. *Phys. Rev. X* **2022**, *12*, 011003.
(76) Levi-Civita, M.-D.-T. Nozione di parallelismo in una varieta qualunque e conseguente specificazione geometrica della curvatura Riemanniana. *Rend. Cir. Mater. Palermo* **1916**, *42*, 173−204.
(77) Persico, E. Realizzazione cinematica del parallelismo superficiale. *Atti R. Acc. Linc. Rend. Cl. Sci. Mater. Fis. Nat.* **1921**, *30*, 127−128.
(78) Pfister, F. Spatial point contact kinematics and parallel transport. *Proc. Inst. Mech. Eng. C: J. Mech. Eng. Sci.* **2002**, *216*, 33−45.
(79) Berry, M. Anticipations of the geometric phase. *Phys. Today* **1990**, *43*, 34−40.
(80) Thurston, W.-P.; Weeks, J.-R. The mathematics of three-dimensional manifolds. *Sci. Am.* **1984**, *251*, 108−121.
(81) Kralj, S.; Rosso, R.; Virga, E.-G. Curvature control of valence on nematic shells. *Soft Matter* **2011**, *7*, 670−683.
(82) Virga, E.-G. Curvature potentials for defects on nematic shells. *Lecture notes*; Isaac Newton Institute for Mathematical Sciences: Cambridge, 2013.
(83) Afghah, S.; Selinger, R.-L.-B.; Selinger, J.-V. Visualising the crossover between 3D and 2D topological defects in nematic liquid crystals. *Liq. Cryst.* **2018**, *45*, 2022−2032.
(84) Nikkhou, M.; Škarabot, M.; Čopar, S.; Ravnik, M.; Žumer, S.; Muševič, I. Light-controlled topological charge in a nematic liquid crystal. *Nat. Phys.* **2015**, *11*, 183−187.
(85) Harkai, S.; Cordoyiannis, G.; Susser, A.-L.; Murray, B.-S.; Ferris, A.-J.; Rožič, B.; Kutnjak, Z.; Rosenblatt, C.; Kralj, S. Manipulation of mechanically nanopatterned line defect assemblies in plane-parallel nematic liquid crystals. *Liq. Cryst. Rev.* **2022**, 1.
(86) Wilczek, F. Majorana returns. *Nat. Phys.* **2009**, *5*, 614−618.
(87) Jagodič, U. Formation of Topological Defects in Liquid Crystal Systems of Non-trivial Geometry. Doctoral Dissertation, 2019.
(88) Vasin, M.-G.; Ryzhov, V.-N.; Vinokur, V.-M. Berezinskii-Kosterlitz-Thouless and Vogel-Fulcher-Tammann criticality in XY model. *arXiv preprint* **2017**, arXiv:1712.00757.
(89) Petridis, L.; Terentjev, E.-M. Nematic-isotropic transition with quenched disorder. *Phys. Rev. E* **2006**, *74*, 051707.
(90) Helfrich, W. Elastic properties of lipid bilayers: theory and possible experiments. *Z. Naturforsch. C* **1973**, *28*, 693−703.
(91) Deuling, H.-J.; Helfrich, W. Red blood cell shapes as explained on the basis of curvature elasticity. *Biophys. J.* **1976**, *16*, 861−868.

https://doi.org/10.1021/acsomega.2c07174
ACS Omega 2023, 8, 169−179